

A Comparison between Three Air Blast Simulation Techniques in LS-DYNA

Hugo Bento Rebelo, Corneliu Cismaşiu

CERIS, ICIST, and Departamento de Engenharia Civil, Faculdade de Ciências e Tecnologia, Universidade NOVA de Lisboa

1 Abstract

When simulating structures subjected to the effects of blast loading, one might resort to three different methods of simulation. These methods are the empirical blast method, also known as Load Blast Enhanced (LBE), the Arbitrary Lagrangian Eulerian (ALE) method, and a coupling method that allows the application of empirical blast loads on air domain simulated with the ALE formulation. Furthermore, for the ALE method, both a mapping technique, that allows the mapping of data from 2D ALE simulations to 2D and 3D ALE meshes, and a complete 3D ALE simulation could be performed.

In order to verify and compare the efficiency and accuracy of these air blast methods, an air blast loading on a reinforced concrete slab is modelled. Additionally, mesh convergence studies of 2D and 3D ALE simulations are performed.

2 Test description

The created numerical model was based on a full-scale blast experimental test presented by Gonçalves [1]. This test, part of the *Strategic building structural security and integrity against accidental or deliberate explosions* (SI4E) research project [2], was designed to evaluate the response of a reinforced concrete one-way slab against blast loads.

For this test, the explosive charge, 8 kg of TNT, was suspended 3 m above the slab top surface, aligned with its centre, as illustrated in Figure 1.

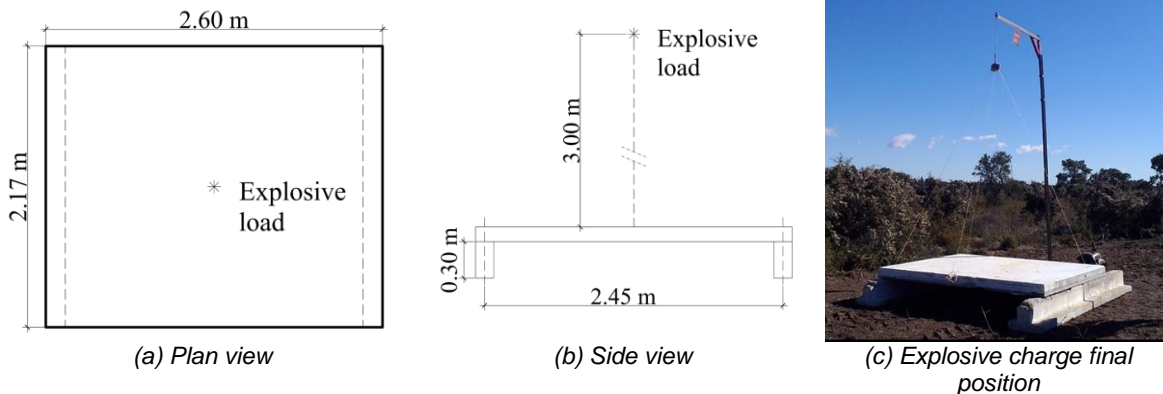


Fig.1: Blast test setup

Considering the symmetry of the test, and in order to reduce computational time and allow for a higher refinement of the mesh, only a quarter of the experimental model was modelled, as shown in Figure 2. The concrete was discretized using a Lagrangian mesh of eight-node solid hexahedron elements with constant stress. To avoid zero energy modes, due to the reduced integration elements, the Flanagan-Belytschko stiffness form hourglass control was applied with the coefficient set to 0.025.

The material model used to simulate the concrete's behaviour is the ***MAT72R3** implemented in LS-DYNA. On the other hand, Hughes-Liu beam elements, in combination with the ***MAT_PIECEWISE_LINEAR_PLASTICITY** material model, were used to model steel reinforcement. The embedment of reinforcement into the concrete Lagrangian mesh was achieved via the ***CONSTRAINED_LAGRANGE_IN_SOLID** keyword (CTYPE = 2).

The boundary conditions necessary to correctly replicate the experimental conditions are represented in Figure 2. These conditions include the addition of the reinforced concrete support, fixed at its base, and the application of symmetry constrains. Lastly, the simulation of contact between the support and the slab was performed through the `*AUTOMATIC_SURFACE_TO_SURFACE` keyword available in LS-DYNA.

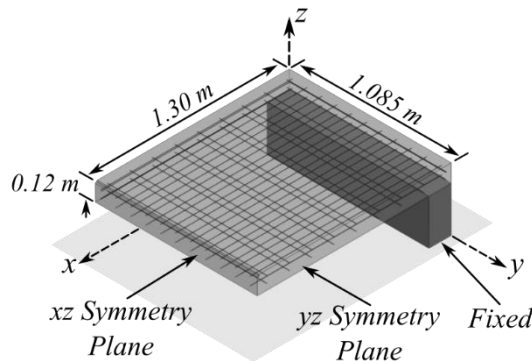


Fig.2: Geometry and boundary conditions of the Lagrangian model

3 Empirical Blast Load

The empirical blast loading is generated through `*LOAD_BLAST_ENHANCED` (LBE) keyword given in LS-DYNA. This method is based on the implementation of the Kingery and Bulmash experimental TNT data [3] performed by Randers-Pehrson and Bannister [4]. The top face of the model is selected to receive pressure resulting from the blast load. From this information, and the location and weight of the charge, the air blast function determines the appropriate pressure time history.

Section 6 presents the estimates obtained with the LBE method, when an 8 kg TNT charge located 3 m above the centre of the slab is considered, both in terms of pressure time history and impulse time history.

3.1 Slab mesh sensitivity analysis

In order to ensure the numerical stability of the results, while maintaining a reasonable time of analysis, a mesh sensitivity analysis was performed. This analysis was carried out through the evaluation of the maximum displacement at the centre of the slab resulting from the application of the aforementioned blast load. Note that, the Lagrangian part of the model is required in all the methods.

During this process, the number of elements in z direction, which corresponds to the thickness of the slab, was successively increased and, in order to simplify the process, the number of elements used in the remaining directions was computed to maintain a cubic geometry. Additionally, the number of elements used in the support's longitudinal direction, y , was equal to the number of elements used in the slab. Lastly, for the reinforcement bars, the same number of divisions was used in the respective direction.

Table 1 collects, for each refinement, the mesh size used in each direction, as well as the resultant number of nodes used in the model of the slab, including the nodes necessary to model the reinforcement bars.

Table 1: Mesh details of the Lagrangian part of the numerical model

Mesh	Mesh size (mm)						No. of Nodes
	Slab			Support			
	x	y	z	x	y	z	
1	20	20	20	19	20	20	39,108
2	13	12	12	13	12	13	138,668
3	10	10	10	10	10	10	250,295

In Figure 3, one can observe the normalized maximum displacement at the centre of the slab, defined as $\delta_{\max}^i / \max(\delta_{\max}^{i=1:3})$, obtained with each mesh refinement and conclude that *Mesh 2* leads to reliable and accurate results with reasonable computational effort.

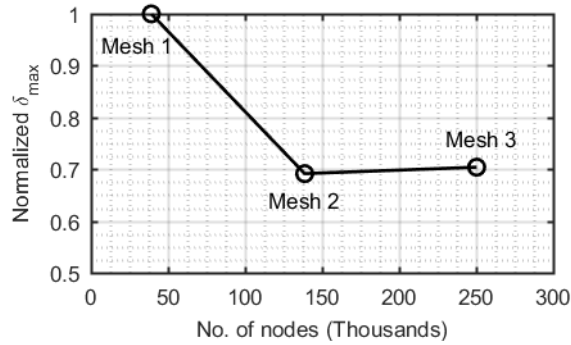


Fig.3: Lagrangian model mesh sensitivity results

4 Arbitrary Lagrangian Eulerian (ALE)

The ALE method is a combined Lagrangian, in which the mesh moves with the material, and Eulerian computing method. This is achieved through the separation of a computation cycle into a Lagrangian phase and a possible advection phase, in which the mesh is either not advected (pure Lagrangian formulation), advected to the original shape (pure Eulerian formulation), or advected to some more advantageous shape [5].

For the present case, the Eulerian Multi-Material (MMALE) formulation was used. In this formulation the materials are allowed to flow through the fixed mesh and each mesh element may contain more than one ALE material. Due to the presence of detonation products, the Donor Cell with Half-Index-Shift advection algorithm (METH = 3) was used. This algorithm is first order accurate and conserves the total energy over each advection step instead of conserving internal energy [6].

The ambient air was modelled with the ***MAT_NULL** card in combination with the linear polynomial Equation of State (EOS), presented in Eq. (1), where the pressure P is expressed as a function of E , the internal energy of air, and $\mu = (\rho / \rho_0) - 1$, where ρ and ρ_0 are the current and reference state densities, respectively.

$$P = C_0 + C_1 \cdot \mu + C_2 \cdot \mu^2 + C_3 \cdot \mu^3 + (C_4 + C_5 \cdot \mu + C_6 \cdot \mu^2) \cdot E \quad (1)$$

The linear polynomial EOS may be used to model air with the gamma law EOS, presented in Eq. (2), by setting every constant C_i to 0, except $C_4 = C_5 = \gamma - 1$, as defined in [6]. All parameter assumed for air under the ***MAT_NULL** and ***EOS_LINEAR_POLYNOMIAL** keywords are collected in Table 2.

$$P = (\gamma - 1) \frac{\rho}{\rho_0} E \quad (2)$$

The explosive material (TNT) was modelled using the ***MAT_HIGH_EXPLOSIVE_BURN** card, whose material parameters are illustrated in Table 2, in combination with the Jones-Wilkins-Lee (JWL) EOS:

$$P = A \left(1 - \frac{\omega}{R_1 V} \right) e^{-R_1 V} + B \left(1 - \frac{\omega}{R_2 V} \right) e^{-R_2 V} + \frac{\omega E}{V} \quad (3)$$

Eq. (3) gives the pressure P as a function of the ratio between the density of the explosive and that of the detonation products V and the detonation energy of the explosive E . Additionally, A , B , R_1 , R_2 and ω are parameters defined in [7] that depend on the used explosive material. Their values are presented in Table 2.

Table 2: Material and EOS input data

Material	Units (m, kg, s)								
Air	*MAT_NULL								
	ρ			Pressure cutoff, PC			Dynamic viscosity, μ		
	1.29			0.0			0.0		
	*EOS_LINEAR_POLYNOMIAL								
	C_0	C_1	C_2	C_3	C_4	C_5	C_6	E_0	V_0
0.0	0.0	0.0	0.0	0.4	0.4	0.0	2.5E+05	1.0	
TNT	*MAT_HIGH_EXPLOSIVE_BURN								
	ρ			Detonation velocity, D			Chapman-Jouget pressure, PCJ		
	1590.0			6930.0			2.1E+10		
	*EOS_JWL								
	A	B	$R1$	$R2$	ω	E_0	V_0		
3.712E+11	3.231E+09	4.15	0.95	0.30	7.0E+09	1.0			

The initial distribution of air and TNT is defined by the ***INITIAL_VOLUME_FRACTION_GEOMETRY** keyword, through the definition of the initial shape and location of the TNT explosive charge. Afterwards, the detonation is initialised using the ***INITIAL_DETONATION** keyword, with the detonation point set at the centre of the explosive charge.

Due to the heavy computational costs of the ALE method, it is not admissible to extend the boundaries of the surrounding air domain too far beyond the outer lines of the Lagrangian part. However, this can result in spurious reflections of the pressure waves at the boundaries of the air domain.

To surpass this problem, the ***BOUNDARY_NON_REFLECTING** card was applied to all surfaces of the air domain, except the bottom surface and the planes of symmetry, as illustrated in Figure 4(a). Additionally, as observed in the experimental test, the presence of the ground generates reflections that need to be considered. Hence, the nodes at the bottom surface of the air domain were fixed. Lastly, the pressure at the ALE mesh boundaries was set to atmospheric pressure via the ***CONTROL_ALE** card.

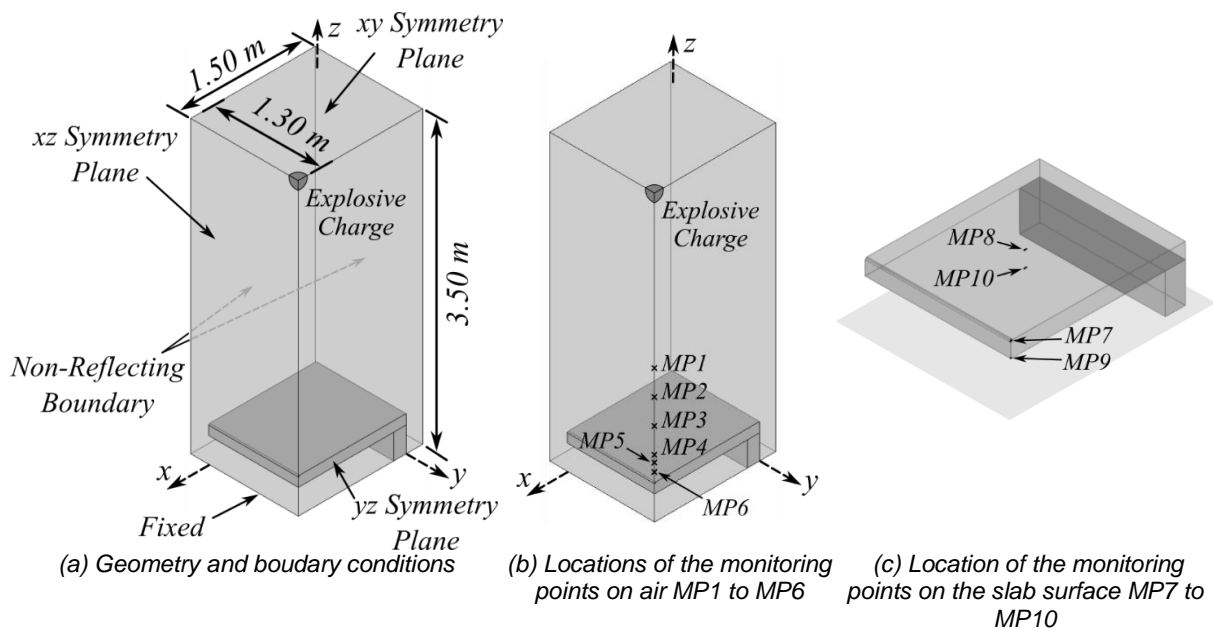


Fig.4: 3D ALE model

Interaction between the air (fluid) and the Lagrangian parts (solids) is accomplished with a penalty-based method activated using the ***CONSTRAINED_LAGRANGE_IN_SOLID** keyword. This method conserves the total energy of the system and applies nodal forces explicitly by tracking the relative motion of a given point [8]. Hence, when a fluid particle penetrates a Lagrangian element, a penalty force, which is proportional to the amount of penetration, is applied to both the fluid particle and the Lagrangian node to prevent penetration [6].

4.1 3D ALE mesh sensitivity analysis

As previously stated, a mesh sensitivity analysis is very important to ensure the numerical stability of the results, which must be obtained within a reasonable time of analysis. Hence, a mesh sensitivity of the ALE mesh was performed, while maintaining the Lagrangian mesh of the slab invariable. In Table 3, one can observe the mesh size used to divide the air domain and the analysis time to run the dynamic analysis for 0.01 s.

Table 3: 3D ALE model mesh details

Mesh	Mesh size (mm)			No. of ALE Elements	Analysis Time
	x	y	z		
1	20	20	20	833,625	04:30:49
2	15	13	15	2,280,000	10:45:44
3	12	10	12	4,631,250	21:18:17

To evaluate the influence of the mesh size, measuring points MP1 to MP6 were positioned in the 3D ALE model, as represented in Figure 4(b), through the ***DATABASE_TRACER** keyword. Additionally, measuring points MP7 to MP10 were placed on the surface of the slab, as illustrated in Figure 4(c), by defining a ***SEGMENT_SET**, which is, afterwards, inserted into the ***DATABASE_FSI** keyword. Note that measuring points MP7 and MP8 are on the top surface of the slab, while measuring points MP9 and MP10 are on the bottom surface.

A comparison between the impulse estimates for the three meshes is presented in Figure 5. Note that the incident impulse, Figures 5(a) to 5(f), obtained with the 3D ALE model, is disturbed by the blast wave reflection on the slab, which leads to a second peak of overpressure and a subsequent increase of impulse. However, this phenomenon is present in all 3 models and it is not significant for the current analysis.

Observing Figure 5, one can conclude that the estimates obtained by using the three meshes are very similar and an additional mesh refinement might be necessary (Figure 5(f), 5(g) and 5(i)). However, in order to maintain 2 or 3 coupling points per each ALE element width, as recommend by [6], NQUAD would have to be increased, which would increase the already heavy computational costs of the method.

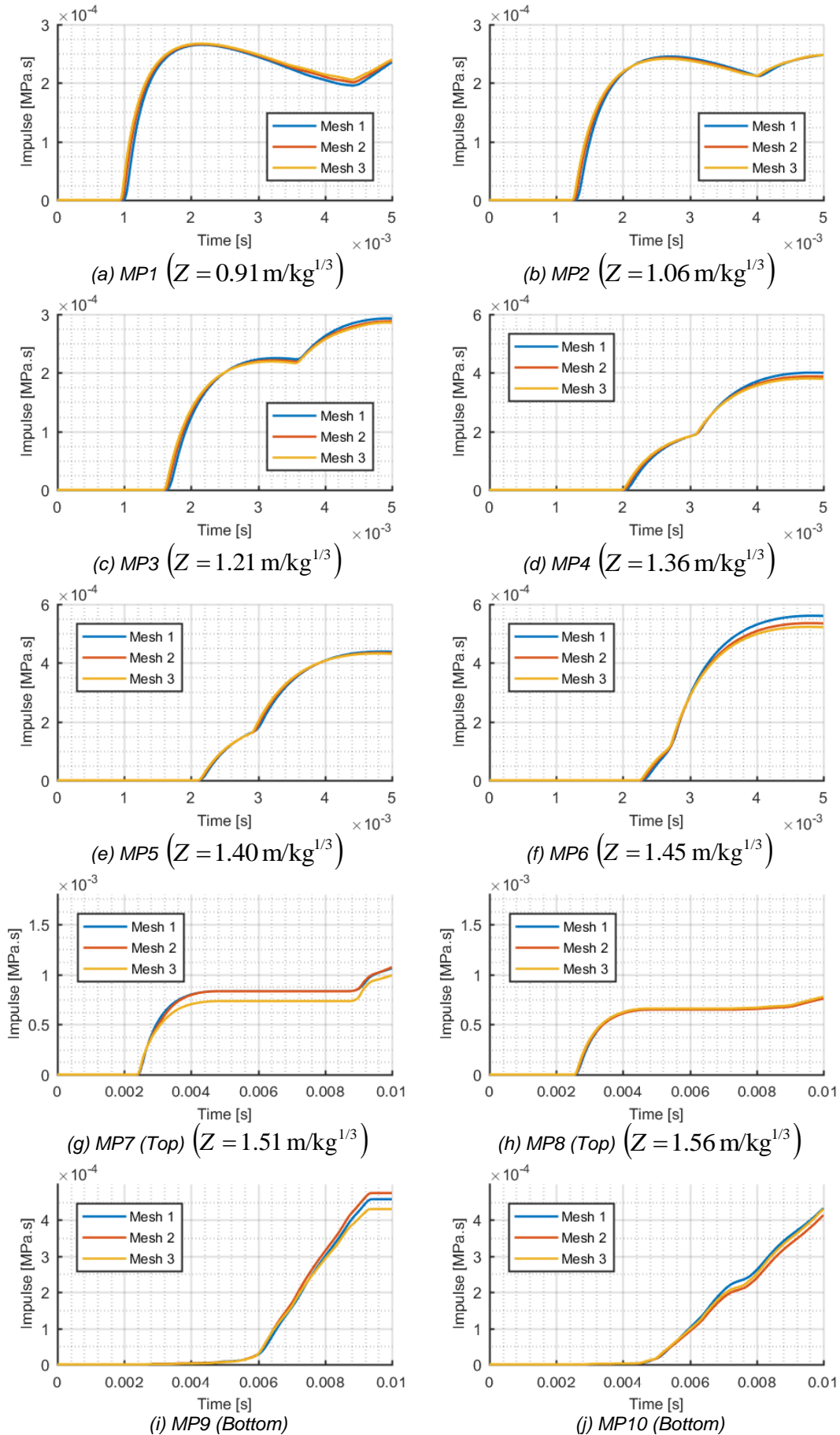


Fig.5: Impulse 3D ALE model

4.2 Mapping from 2D to 3D

To save computational time and increase the accuracy of the results, a technique that allows the mapping of results from 2D to 3D Eulerian domains has been available in LS-DYNA since V971 R4 [9]. Usually, an axisymmetric simulation in 2D is performed until the velocity field is close to the boundary. At the last cycle, a binary map file is written, which contains the variables of the 2D Eulerian domain, and then used to fill the 3D Eulerian domain. Both the use of similar element size in 2D and 3D [8] and the sensitivity from an initial fine element size to a subsequent coarser element size [10] when using the mapping technique have been investigated. It was concluded that the specific impulse remains relatively constant until the element size ratio between the 2D and 3D of 20. However, using a fine mesh for the initial 2D simulation and a coarse mesh for the subsequent 3D simulation will result in improved accuracy, when compared to a single 3D simulation with the same coarse mesh.

As illustrated in Figure 4(a), the smallest dimension of the air domain has 1.30 m, hence an axisymmetric simulation with 1.30×1.30 m, represented in Figure 6(a), was performed. As performed in the 3D ALE model, the Donor Cell with Half-Index-Shift advection algorithm was used. On the other hand, 2D elements with an area weighted formulation were used in this model. The 2D simulation runs to its end time 0.00045 s, when a binary map file is written and the solution is sequentially mapped into the 3D MMALE mesh as an initial condition, as presented in Figure 6(b). Next, the analysis continues using the 3D mesh.

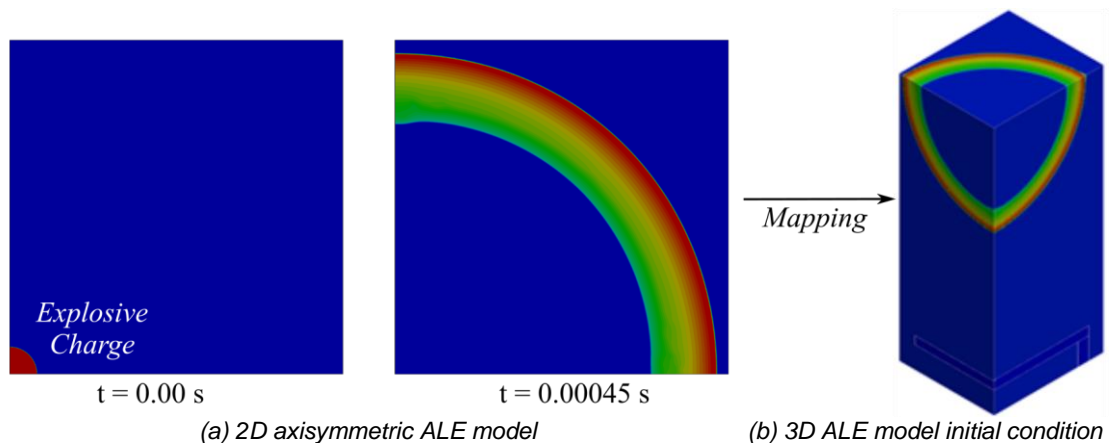


Fig.6: Schematic picture of the initial 2D model and subsequent 3D model after mapping

4.2.1 2D ALE mesh convergence study

According to Schwer [11], the rule-of-thumb is the use of at least 10 elements across the radius of the charge, while 20 is a reasonable number. As the explosive charge radius is 106.3 mm, the performed mesh convergence study was initialized with square elements of 10 mm, and successively divided in half, as presented in Table 4, until convergence was observed. In Figure 7, one can observe the normalized maximum impulse at various distances from the centre of the explosive charge along the axisymmetric axis, and conclude that *Mesh 4*, despite the higher difference in the point at a distance of 1.2 m, reaches reliable results with reasonable computational effort. Additionally, the 1.25 by 1.25 mm 2D elements included over 80 elements across the charge radius, surpassing the value recommend by Schwer [11], while maintaining the ratio between the 2D and all the 3D model meshes under 20 to avoid energy loss between the 2D and 3D models [10].

Table 4: 2D ALE model mesh details

Mesh	Mesh size (mm)	No. of ALE Elements	Analysis Time
1	10×10	16,900	00:00:19
2	5×5	67,600	00:01:54
3	2.5×2.5	270,400	00:18:05
4	1.25×1.25	1,081,600	02:15:22
5	0.625×0.625	4,326,400	18:50:38

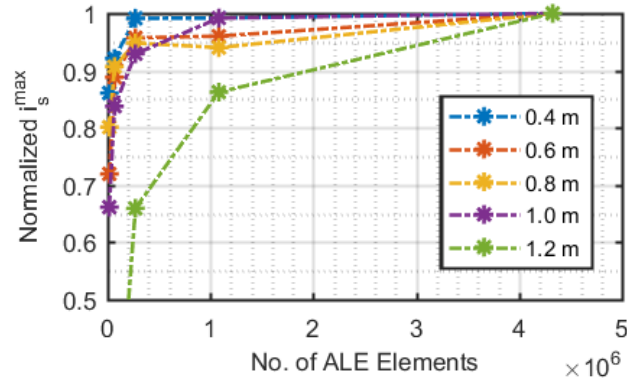


Fig.7: Dependence on the mesh of the normalized maximum impulse at various distances in y direction

4.2.2 3D ALE model results with mapping technique

Figure 8 represents the impulse obtained with the initial detonation in Mesh 3, and the impulse obtained with the mapping from the 2D simulation into Mesh 1, 2 and 3 in *Map Mesh 1*, *Map Mesh 2* and *Map Mesh 3*, respectively. Analysing Figures 8(a) to 8(f), one can verify that the use of the mapping results in higher accuracy for the free-air blast wave propagation, regardless of the mesh used in the 3D ALE model.

Nonetheless, despite the conclusions obtained for the propagation of the free-air blast wave, one must also analyse the impulse that is applied to the slab, as it will influence the structural response. It is possible to observe the resulting impulse at the measuring points on the slab in Figure 8(g) to 8(j).

Figure 9(a) presents the average pressure time history considering both the top and bottom surfaces of the slab. The resulting impulse was obtained by integrating the average pressure time history with respect to time and illustrated in Figure 9(b). Additionally, Table 5 collects the total analysis time and the estimate for the maximum impulse obtained by each model.

Analysing Figure 9(b) and Table 5, it is possible to verify that the 3D ALE model with Mesh 1, in combination with the mapping technique, is capable to estimate the propagation of the blast wave and subsequent interaction with the slab with approximately the same precision as the 3D ALE model with Mesh 3, in combination with the mapping technique, while taking approximately one third of the analysis time.

Table 5: Resulting analysis time

3D Mesh after Mapping	Total Analysis Time (Mapping + 3D Model)	Maximum Impulse [Pa.s]
1	07:10:59	553.61
2	13:49:33	556.66
3	24:51:05	553.62

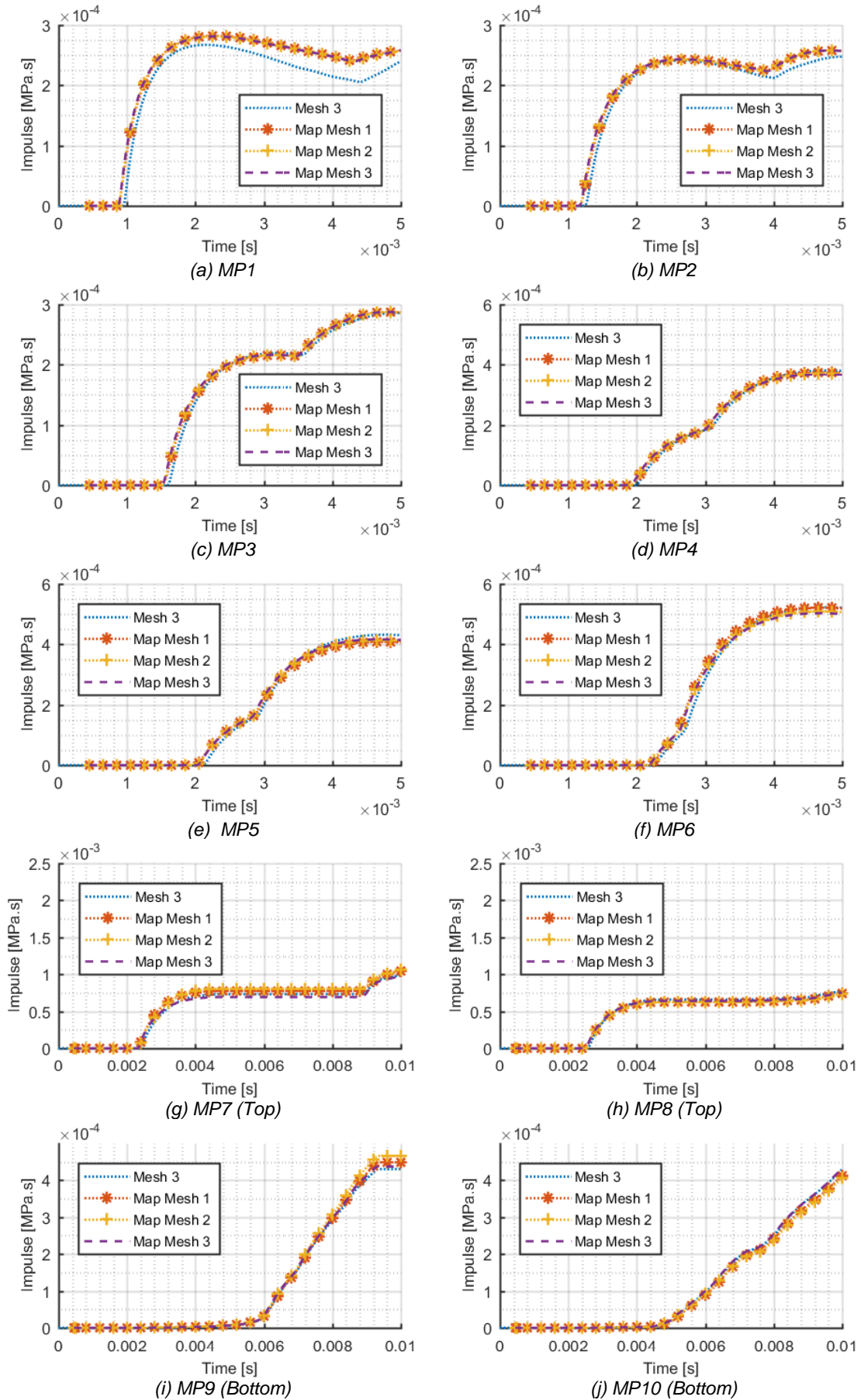


Fig.8: Impulse 3D ALE model with mapping technique

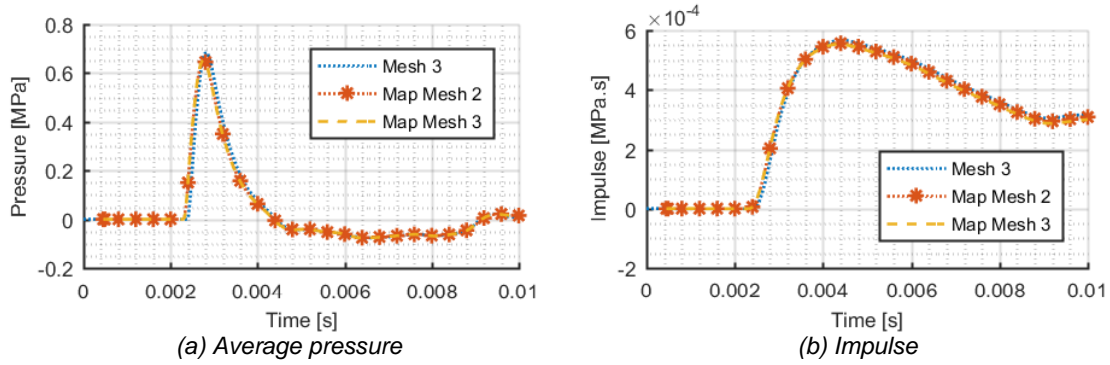


Fig.9: Average pressure and resulting impulse 3D ALE model with mapping technique

5 Coupling the LBE to ALE

In the present method, empirical blast loads, presented in Section 3, are applied to the air domain simulated with the MMALE formulation, offering several advantages over the use of either technique for air blast simulations [12, 13]. Although computationally efficient, the LBE approach requires a clear line of sight between the charge and the target structure. Furthermore, the focusing of blast wave energy due to the merging of waves after reflecting off structures is not considered. In contrast, MMALE formulation requires a large air domain and a relatively fine mesh to adequately resolve the air shock, which lead to a large computational burden.

With the presented technique, which is a combination of the two aforementioned methods, the air surrounding the intervening structures is modelled with an ALE domain, while the blast pressures are provided by the empirical values, implemented in `*LOAD_BLAST_ENHANCED`, and applied to a layer of ALE elements, commonly known as ambient layer. Afterwards, the blast wave propagates through the air domain. Hence, theoretically, the strengths of each method are preserved and combined to allow the simulation of long standoffs, without modelling huge air domains, while maintaining the ability to simulate shadowing and focusing [12].

As performed for the 3D ALE model, the boundary conditions due to the quarter-symmetry were enforced in the respective boundaries of the air domain, while the remainder exterior surfaces were treated as non-reflecting boundaries. All parameters and definitions of air and EOS are equal to the pure 3D ALE model in both the air domain and ambient layer. Nonetheless, the ambient layer must be activated by setting `AET=5` in `*SECTION_SOLID`. Later, the exterior segments of the ambient layer are identified in `*LOAD_BLAST_SEGMENT`, where one must set the parameter `ALEPID` equal to the part number of the ambient elements. The model used to simulate the air blast experiment with the coupling method is represented in Figure 10, while the mesh details are tabulated in Table 6. The results obtained with the present method are shown in Section 6.

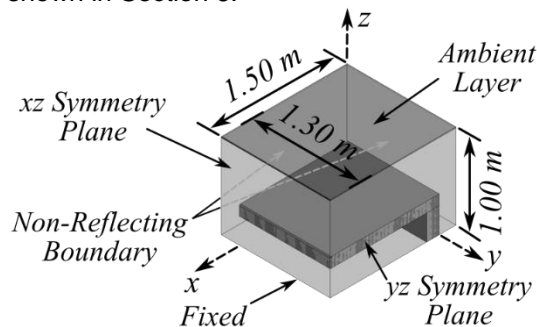


Fig.10: Geometry and boundary conditions of the 3D LBE ALE model

Table 6: 3D LBE ALE model mesh details

Domain	Mesh size (mm)			No. of ALE Elements	Analysis Time
	x	y	z		
Air	20.0	20.0	20.0	243,750	02:26:53
Ambient	20.0	2	10.0	4,875	

6 Comparison of results

The present section aims to present and compare the air blast loading on a reinforced concrete slab obtain with the reviewed methods.

The incident impulse on monitoring points MP5 and MP6, obtained with the three air blast methods, is illustrated in Figure 12, from which one can observe that, before the increase of impulse due to the blast wave reflection on the slab, the LBE and the coupling of LBE with ALE lead to similar impulses, which are higher than the impulse obtained with the ALE method. This higher incident impulse, computed with the coupling of LBE with ALE, results in larger reflected impulses at the monitoring points located on the top surface of the slab, Figures 12(b) and 12(d), while the impulses registered on the bottom surface of the slab are similar, as visualized in Figures 12(f) and 12(h).

Lastly, as previously reviewed, the LBE air blast method does not have the capacity to apply pressure to the bottom surface of the slab,

Taking into account the aforementioned notes, and observing Figure 13, one can verify that the maximum impulse, obtained with the coupling of LBE with ALE is higher than the maximum impulse obtained with the LBE method, despite the absence of pressure on the bottom surface of the slab on the latter. It is also higher than the maximum impulse estimated by the ALE method, due to the higher impulse applied to the top surface of the slab, as observed in Figures 14(b) and 14(d).

Lastly, from Table 7, it is possible to observe that the ALE method took approximately the triple of the time to complete the analysis than the coupling method and 70 times more time than the Lagrangian formulation.

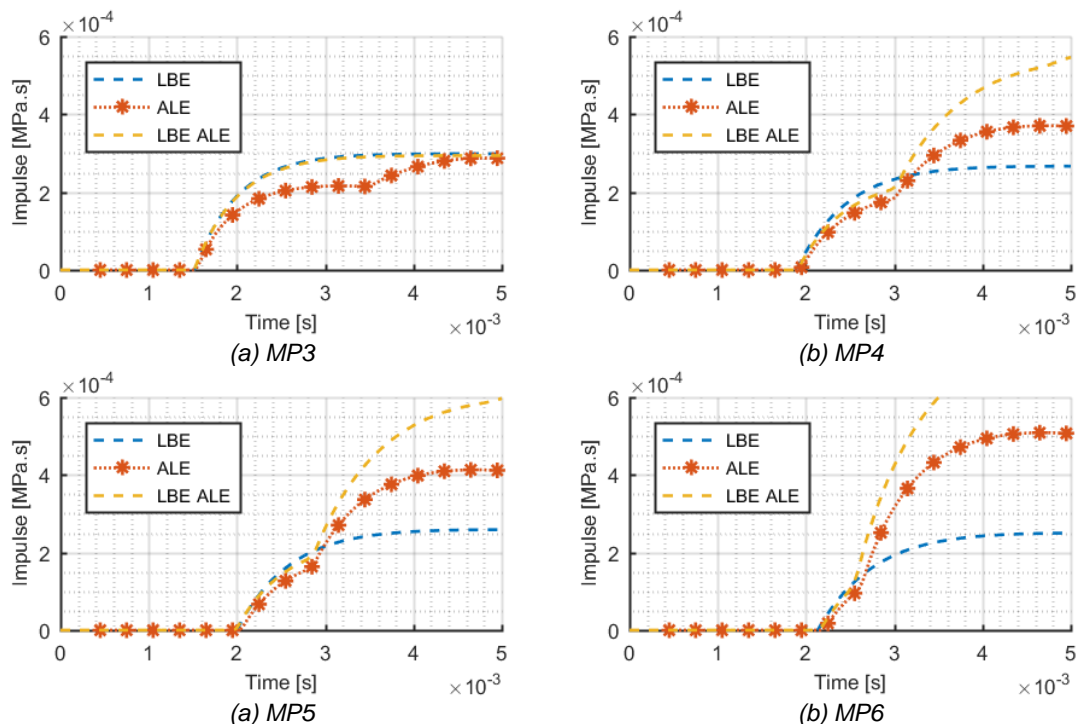


Fig.11: Comparison of incident impulse obtained with the air blast methods

Table 7: Summary of results obtained with the different air blast methods

Method	No. of ALE Elements	Analysis Time	Maximum Average Pressure [MPa]	Maximum Impulse [Pa.s]
LBE	0	00:06:09	0.71	602.60
ALE	833,625	07:10:59	0.64 (-9.54%)	553.61 (-8.13%)
Coupling	248,625	02:26:53	0.75 (5.80%)	724.30 (20.15%)

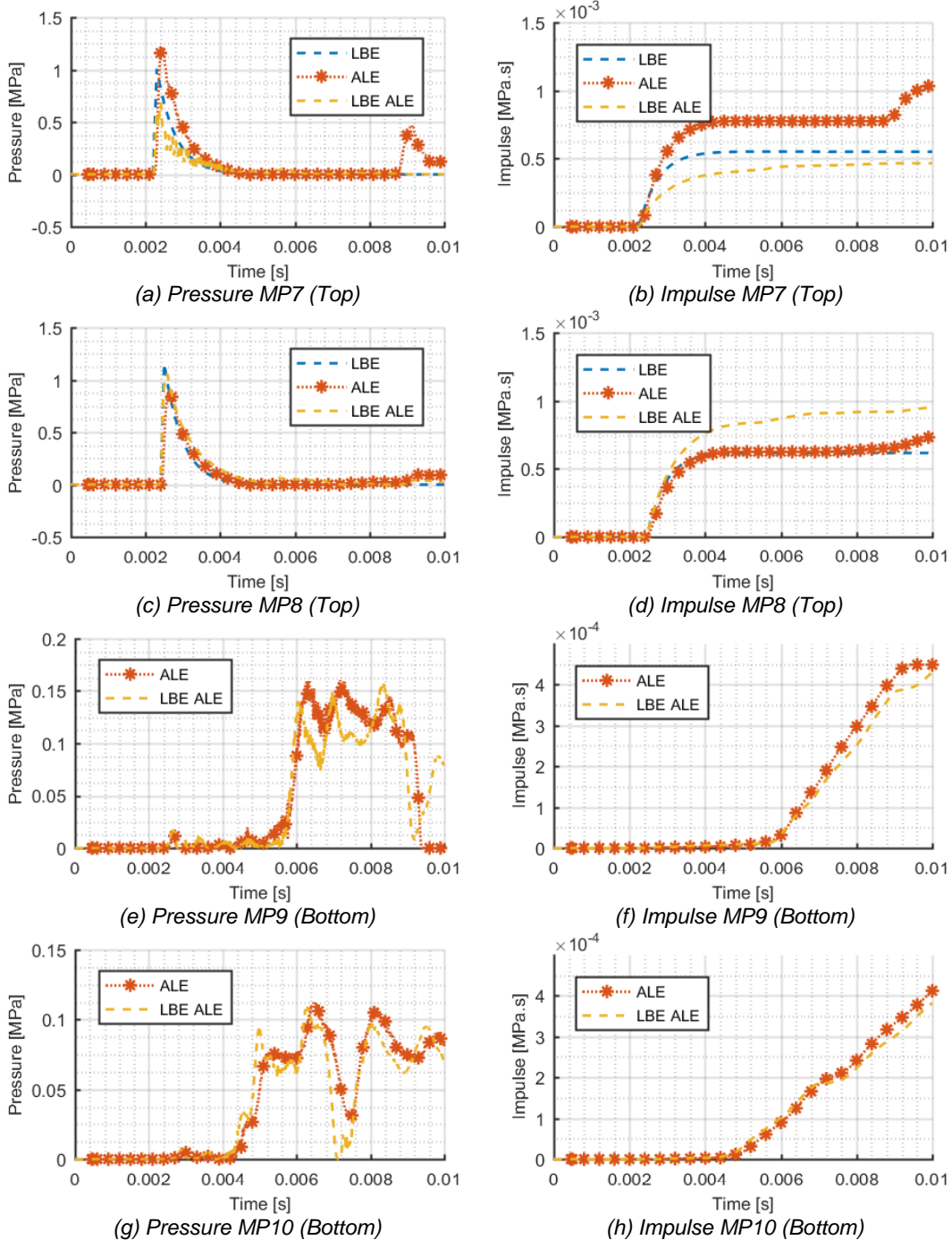


Fig. 12: Comparison of reflected pressure and impulse obtained with the air blast methods

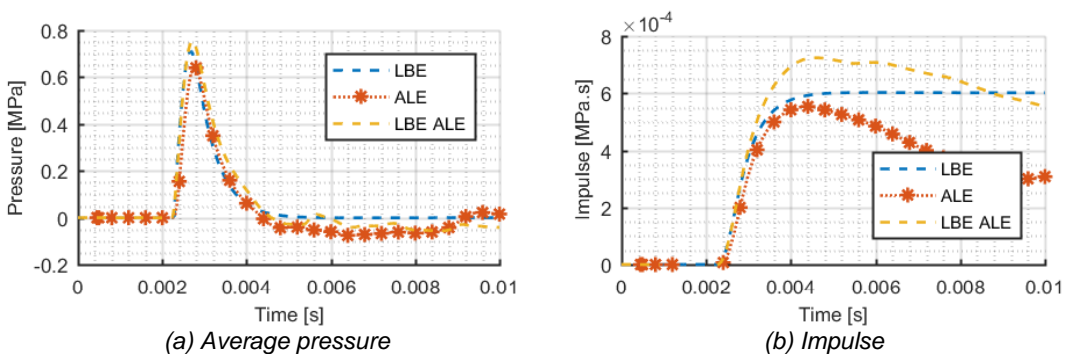


Fig. 13: Comparison of average pressure and resulting impulse obtained with the air blast methods

7 Summary

The present paper aimed to present and compare the results obtained with three air blast methods, when an air blast loading on a reinforced concrete slab is modelled. These methods are the Load Blast Enhanced (LBE) method, the Arbitrary Lagrangian Eulerian (ALE) method, and a coupling method that allows the application of empirical blast loads on air domain simulated with the ALE formulation.

As expected, the most efficient method, in terms of computational effort, is the pure Lagrangian method, or LBE method. However, this method does not consider shadowing and focusing of the blast waves due to the presence of structures.

On the other hand, when compared with the LBE method, the coupling between the empirical blast loads and the ALE formulation, conducted to a higher maximum impulse, while the ALE method resulted in a smaller maximum impulse.

Furthermore, for the ALE method, the reviewed mapping technique, that allows the mapping of data from 2D ALE simulations to 2D and 3D ALE meshes, greatly improved the efficiency, while maintaining accuracy, of the ALE method by reducing in one third the analysis time.

8 Literature

- [1] M. Gonçalves, Reforço de Placas de Betão Armado com Argamassas Armadas para Acções de Explosão, Master's Thesis, FCT-UNL: Caparica, 2015.
- [2] CINAMIL Research and Development Projects, [Online]. Available: <http://academiamilitar.pt/investigacao-e-inovacao/projetos.html>. [Accessed 27 03 2017].
- [3] C. Kingery and G. Bulmash, "Air blast parameters from TNT spherical air burst and hemispherical burst," US Army Armament and Development Center, Ballistic Research Laboratory, Aberdeen Proving Ground, Maryland, 1984.
- [4] G. Randers-Pehrson and K. Bannister, "Airblast Loading Model for DYNA2D and DYNA3D," DTIC Document, 1997.
- [5] H. C.W., A. A.A. and J. Cook, "An Arbitrary Lagrangian-Eulerian Computing Method," *Journal of Computational Physics*, no. 14, 1974.
- [6] J. Hallquist, LS-DYNA Keyword User's Manual, California, USA: Livermore Software Technology Corporation (LSTC), 2015.
- [7] B. Dobratz, LLNL Explosives Handbook: Properties of Chemical Explosives and Explosives and Explosive Simulants, California, USA: Lawrence Livermore National Lab, 1981.
- [8] M. Souli and L. Olovson, "Fluid-Structure Interaction in LS-DYNA: Industrial Applications," in *4th European LS-DYNA Users Conference*, Ulm, Germany, 2003.
- [9] N. Aquelet and M. Souli, "2D to 3D ALE Mapping," in *10th International LS-DYNA Users Conference*, Dearborn, USA, 2008.
- [10] V. Lapoujade, N. Van Dorselaer, S. Kevorkian and K. Cheval, "A Study of Mapping Technique for Air Blast Modeling," in *11th International LS-DYNA Users Conference*, Detroit, USA, 2010.
- [11] L. Schwer, H. Teng and M. Souli, "LS-DYNA Air Blast Techniques: Comparisons with Experiments for Close-in Charges," in *10th European LS-DYNA Conference*, Würzburg, Germany, 2015.
- [12] T. Slavik, "A Coupling of Empirical Explosive Blast Loads to ALE Air Domains in LS-DYNA," in *7th European LS-DYNA Conference*, Salzburg, Austria, 2009.
- [13] L. Schwer, "A Brief Introduction to Coupling Load Blast Enhanced with Multi-Material ALE: The best of Both Worlds for Air Blast Simulation," in *LS-DYNA Forum*, Bamberg, Germany, 2010.